Tectonophysics 656 (2015) 202–214

Contents lists available at ScienceDirect

Tectonophysics

journal homepage: www.elsevier.com/locate/tecto

Graviquakes in Italy

P. Petricca [a], S. Barba [b], E. Carminati [c,d], C. Doglioni [c,d,*], F. Riguzzi [b]

[a] GFZ-German Research Centre for Geosciences, Potsdam, Germany
[b] Istituto Nazionale di Geofisica e Vulcanologia, Roma, Italy
[c] Dipartimento di Scienze della Terra, Università Sapienza, Roma, Italy
[d] Istituto di Geologia Ambientale e Geoingegneria, CNR, Roma, Italy

ARTICLE INFO

Article history:
Received 28 March 2015
Received in revised form 15 June 2015
Accepted 1 July 2015
Available online 9 July 2015

Keywords:
Normal fault earthquakes
Graviquakes
Italian seismicity
Seismic volume

ABSTRACT

We discuss the mechanics of crustal normal fault-related earthquakes, and show that they represent dissipation of gravitational potential energy (graviquakes) and their magnitude increases with the involved volume (delimited by the seismogenic fault and an antithetic dilated wedge in its hangingwall), and the fault dip. The magnitude increases with the deepening of the brittle–ductile transition (BDT), which in turn enlarges the involved volume. The fault dip seems rather controlled by the static friction of the involved crustal layers. We apply the model to the extensional area of the Italian peninsula, whose geodynamics is controlled by the Alpine and Apennines subduction zones. The latter has a well-developed backarc basin and a large part of the accretionary prism is affected by on-going extensional tectonics, which is responsible for most of peninsular Italy seismicity. Analyzing the seismic record of the Apennines, the length of seismogenic normal faults tends to be at most about 3 times the hypocenter depth. We compile a map of the brittle–ductile transition depth and, assuming a fixed 45° or 60° fault dip and a dilated wedge developed during the interseismic period almost perpendicular to the fault plane, we compute the maximum volume of the hangingwall collapsing at the coseismic stage, and estimate the maximum expected magnitude. Lower magnitude values are obtained in areas with thinner brittle layer and higher heat flow. Moreover, lower magnitude relative to those theoretically expected may occur in areas of higher strain rate where faults may creep faster due to lower frictional values.

1. Introduction

Earthquakes nucleate where pressure gradients are sufficiently large to overcome rock strength, such as at the boundary between crustal layers having contrasting rheology or at the brittle–ductile transition (BDT). Normal fault-related crustal earthquakes, like all seismic events, are controlled by friction (Marone, 1998; Niemeijer et al., 2010; Ruina, 1983; Schleicher et al., 2010), fluid pressure, strain rate, brittle–ductile transition (BDT) depth, etc. However, unlike earthquakes generated by thrusts (e.g., Cooke and Murphy, 2004) and strike–slip faults, which are fed by elastic energy, normal faults release mostly gravitational potential energy (Dahlen, 1977; Dempsey et al., 2012; Doglioni et al., 2011, 2014; Savage and Walsh, 1978) and for this reason they can be classified as graviquakes (Doglioni et al., 2015b). Since they work in favor of gravity, they show a different mechanical evolution with respect to other seismogenic faults that instead dissipate elastic energy accumulated during the interseismic period to move crustal volumes against (thrust) or at neutral (strike–slip) gravity. The magnitude of graviquakes is mostly controlled by the mass involved in the collapse at the coseismic stage (Fig. 1). The graviquake model proposed here predicts the generation of a dilated wedge, almost perpendicular to the fault plane in the upper brittle crust during the interseismic period, caused by strain partitioning between the steady-shearing mylonitic portion of the shear zone in the lower crust (e.g., Rutter, 1986) and the locked overlying portion of the fault in the upper brittle layer (Fig. 1). When the dilated wedge and the locked brittle portion of the fault cannot sustain anymore the overlying volume, the fall of it will produce the earthquake. The earthquake magnitude increases proportionally to the logarithm of the involved volume and the vertical component of slip along the fault (Fig. 1). Therefore, the bigger the falling mass and the steeper the fault, the larger will result the magnitude. Peninsular Italy, characterized by extensional tectonics and consequent normal faulting-related moderate seismicity, is used as a natural laboratory to test the validity of the graviquake model. In the past, Bath and Duda (1964) have already evidenced an empirical linear correlation between the earthquake magnitudes and the logarithm of the involved volumes.

* Corresponding author at: Dipartimento di Scienze della Terra, Università Sapienza, Roma, Italy. Tel.: +39 06 4991 4549; fax: +39 06 4459 724.
E-mail address: carlo.doglioni@uniroma1.it (C. Doglioni).

http://dx.doi.org/10.1016/j.tecto.2015.07.001
0040-1951/

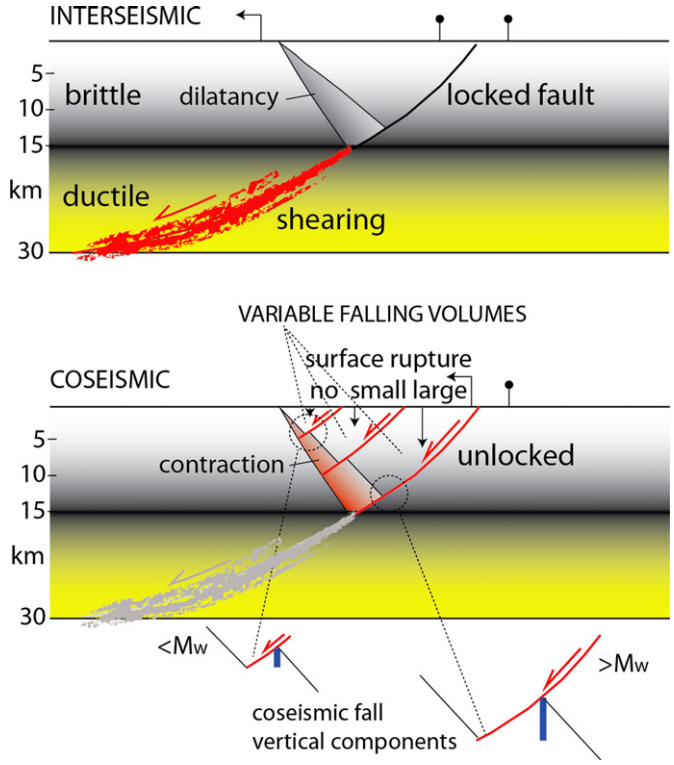

Fig. 1. Geological model of the seismic cycle associated with a normal fault. During the interseismic period, while the lower crust is shearing in a steady state, the brittle upper crust is locked and a dilating wedge is inferred. The coseismic collapse of the hangingwall will recover part of the total extension and it will be a function of the depth of the tip line of the activated normal fault. The deeper the fault, the bigger the falling volume and the larger is the fault displacement. Therefore the deeper the fault, the larger is also the vertical component of the displacement, and the larger will be the magnitude of the earthquake. Since the motion of the hangingwall mostly dissipates gravitational potential energy, we adopt the term graviquakes (Doglioni et al., 2015b).

In their case the volumes were seismologically defined as the portion of space filled by the aftershocks. We follow here a different approach, putting together different pieces of evidence with a multidisciplinary approach.

2. Seismotectonics of Italy

The Apennines formed in the hangingwall of a W-directed and easterly retreating slab (Barba et al., 2008; Carminati and Doglioni, 2012; Carminati et al., 2012). The easterly migration of the subduction system has generated a single verging accretionary prism located in the eastern flank of the Apennines, mostly buried beneath the Po Basin, the western Adriatic Sea and Ionian Sea. The accretionary prism is active as indicated by deformation of Quaternary sediments, seismicity (Fig. 2) and GPS data (Figs. 3 and 4). To the west of it, the Apennines are affected by extensional tectonics associated with backarc rifting, in which the inherited accretionary prism is crosscut by normal faults. Most of the more energetic extensional earthquakes are concentrated along the ridge of the Apennines (Fig. 2), possibly because it is characterized by the thickest and coldest crust, with maximum values of lithostatic load (σ1) at the bottom of the brittle layer (Doglioni et al., 2015a).

2.1. Geodetic constraints

The increased number of GNSS (Global Navigation Satellite System) networks in the Italian area allows more detailed spatial and temporal resolutions of the on-going crustal deformation (Riguzzi et al., 2012, 2013), providing an unprecedent map of intra-plate kinematics of the region (Fig. 3). The current archiving and daily data processing concern 21 different Italian GNSS networks established with different aims and other 50 sites belonging to EUREF and/or IGS networks used for the ITRF2008 reference frame definition. The overall dataset comes from more than 900 GNSS sites, 1998 being the initial recording epoch.

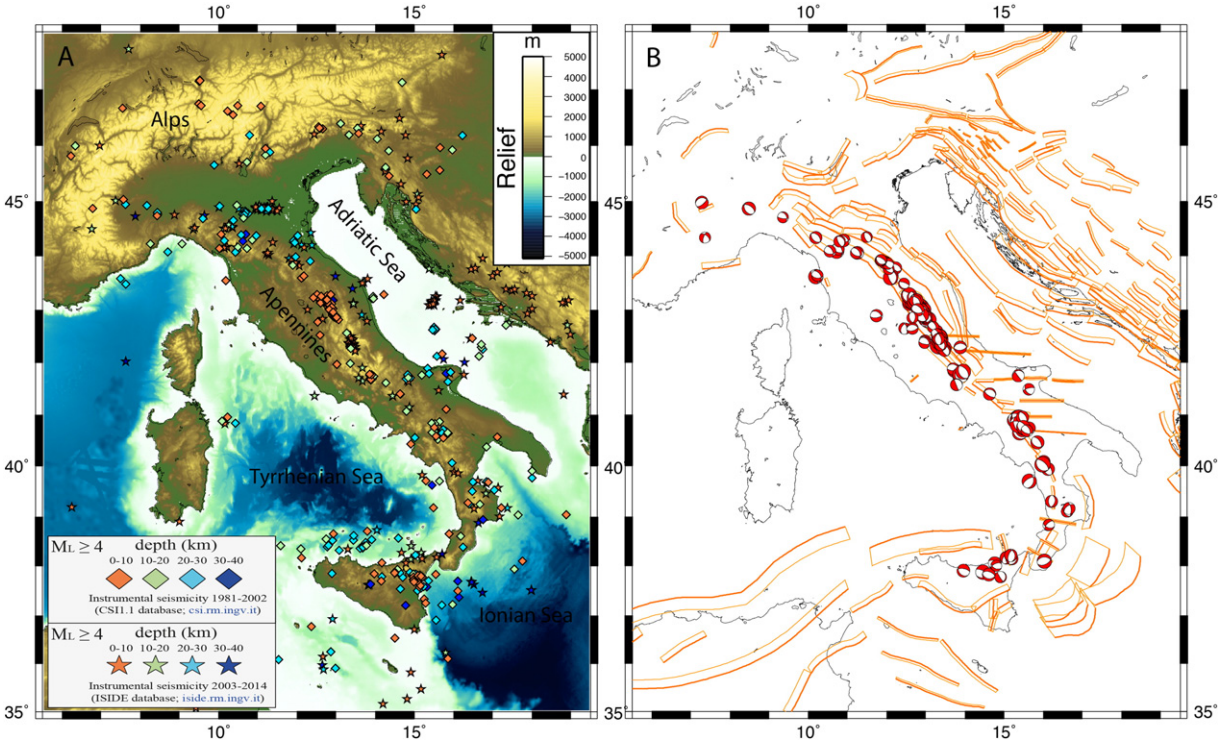

Fig. 2. A) Seismicity of the Italian area and surroundings with M > 4 (1981–2014, from CSI1.1 and ISIDE database). B) Normal fault-related earthquakes along the peninsula and Sicily, and seismogenic faults (M > 5.5) of the DISS and EDSF databases (Basili et al., 2008; Basili et al., 2013). Extensional tectonics can be inferred as related to the easterly retreating Apennines slab and associated backarc basin formation.

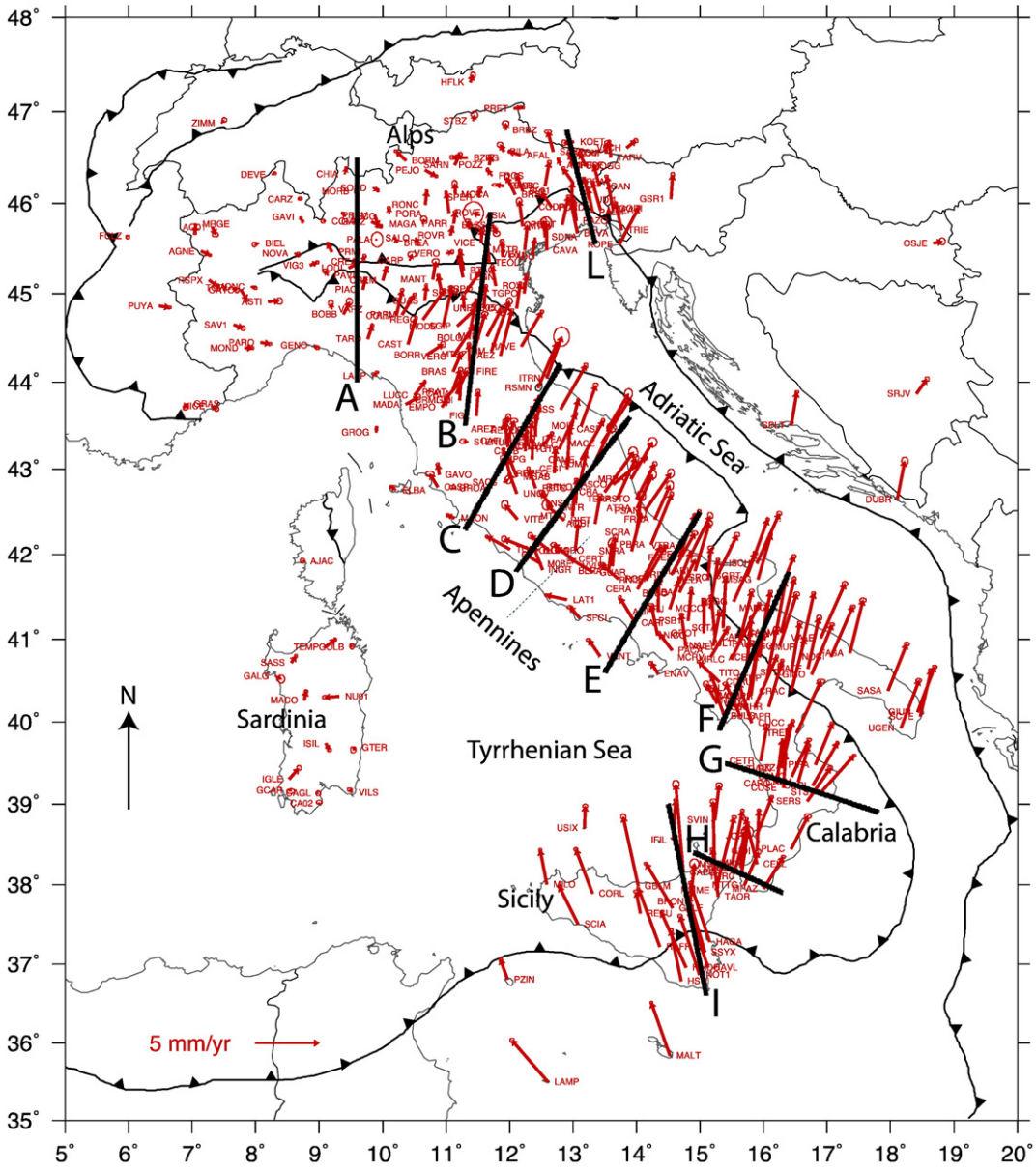

Fig. 3. Horizontal GPS velocity field of sites in Italy and few other stations with respect to Eurasia. Sites with a minimum time span of 4 years are shown. A–L black lines: sections shown in the next figure along which the horizontal velocities of sites located within a distance of 20 km from the line have been projected. Although some movement in the third dimension is certainly present, sections have been traced parallel to the main extensional or contractional regional stress field.

The raw data processing is based on the BPE routine of the Bernese GNSS software v. 5.0 (Beutler et al., 2007), following the processing options of the EUREF Guidelines for EPN Analysis Centres (http://www.epncb.oma.be). The daily solutions are estimated in a loosely constrained reference frame, so that the coordinates result randomly translated or rotated from day-to-day and the covariance matrices are dilated (reaching the order of meters). The ITRF2008 reference frame is then imposed following the procedures described in Devoti et al. (2014), by imposing a 4-parameter similarity transformation (translations and scale factor, Devoti et al., 2010), based on 45 sites located in central Europe as anchor stations. The site velocity components are estimated fitting simultaneously a linear drift, episodic offsets and annual sinusoids to all the coordinate time series (Devoti et al., 2008, 2011, 2014). Offsets are estimated whenever a change in the GPS equipment or an earthquake occurrence induces a significant step in the time series. Seasonal oscillations are accounted for by annual sinusoids. Moreover outliers are rejected whenever the weighted residual exceeds three times the global chi square (χ^2). Finally the common mode error signal is filtered out (Devoti et al., 2014, 2015).

The estimated horizontal velocity field with respect to the Eurasian plate, realized by minimizing the rigid motion of 15 selected EUREF stations located in stable central Europe, is shown in Fig. 3. The formal velocity errors obtained after the inversion have been rescaled site by site with the corresponding normalized variance factors. Each GNSS site spans different life times. Only those with a minimum observation time of 4 years have been here considered. The velocities are projected along the cross-sections shown in Fig. 3, considering only stations located within 20 km from each section (Fig. 4). The red dotted lines provide a raw interpolation of the projected velocities. Up-and-right trends indicate extension and down-and-right trends contraction. Along sections, undulations of the velocity trend (and of the related strain rate) could indicate a variation of friction due to lateral lithological variations (e.g., rheological contrast between carbonate platform rocks having high friction and deeper-water shaly rocks with lower friction). Moreover, the strain rates as along the Alto Tiberina fault (Hreinsdóttir and Bennett, 2009) could indicate creep where the fault crosses evaporites (Fig. 4c, between 75 and 200 km). The pattern of geodetic velocities

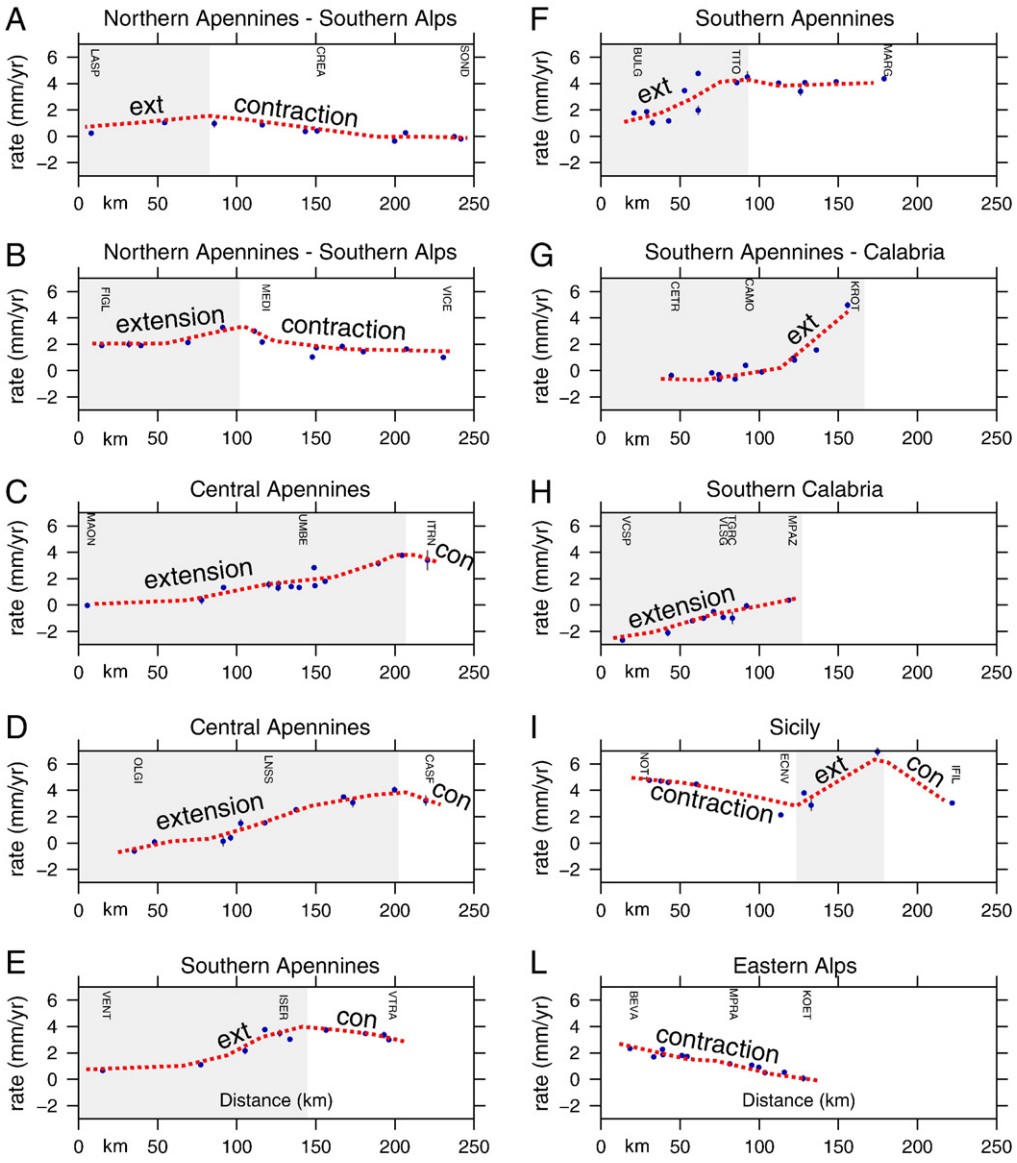

Fig. 4. GPS velocity in mm/year along the cross-sections shown in the previous figure. A–L subsets: projected velocities of all the sites located within 20 km from the line. The red dashed line is an inferred trend of the movement. Rising toward the right indicates extension (ext), whereas decrease means contraction (con). The steeper the line, the faster the velocity. We suggest that gradients in velocity may be controlled also by variations of the mean static friction in the brittle upper crust. The gray segment of the sections represents the on-going extensional part.

allows the distinction of areas with different kinematic behavior. It is proposed that the slower the movement, the higher could be the friction and vice-versa. If so, the higher the friction, the larger is the interseismic stored energy. The seismicity from areas of Italy where GPS data illuminates active extensional tectonics (Figs. 5 and 6) will be used to validate/constrain the proposed model in the next sections. GPS data indicate that extension in the Apennines is not confined along the elevated ridge, but rather distributed all over the western side, at least up to the Tyrrhenian Sea coast (Fig. 4). Thus extension cannot be attributed solely to gravitational spreading of the belt.

The sites of Fig. 3 show vectors oblique to high angle relative to the section traces of Fig. 4. Although sites in the western side of the Apennines show a NW-ward motion and those of the eastern side move NE-ward, these vectors do not represent neither the motion relative to the mantle, nor the relative motion among the single sites. The cross-sections of Fig. 4 are generally parallel to the regional extensional or contractional stress fields and illustrate the rates of motion along the different segments of the Italian peninsula. However, some transtension or transpression can be appreciated in the different tectonic settings.

2.2. Brittle–ductile transition (BDT) and differential stress

In order to quantify the maximum volume that can be mobilized by normal faults in the crustal extensional domain of peninsular Italy and surroundings, we first attempted to compute the depth of the BDT of the region. Based on heat flow (Della Vedova et al., 2001), crustal thickness (Carafa and Barba, 2011; Mele et al., 2013), and composition (quartz rheology for the upper crust and diabase rheology in the lower crust) of the area (although in the Tyrrhenian Sea there are two areas of oceanic crust), we computed the map of the thickness of the brittle layer of the upper crust on a 1 × 1 km grid, covering the whole Italian area, spanning from 5° to 20° longitudes and from 35° to 48° latitudes (Fig. 5). We adopted the following three working steps to construct the map.

First lithospheric thickness and depth to the Moho are evaluated for each node using an up-to-date regional scale dataset mostly based on

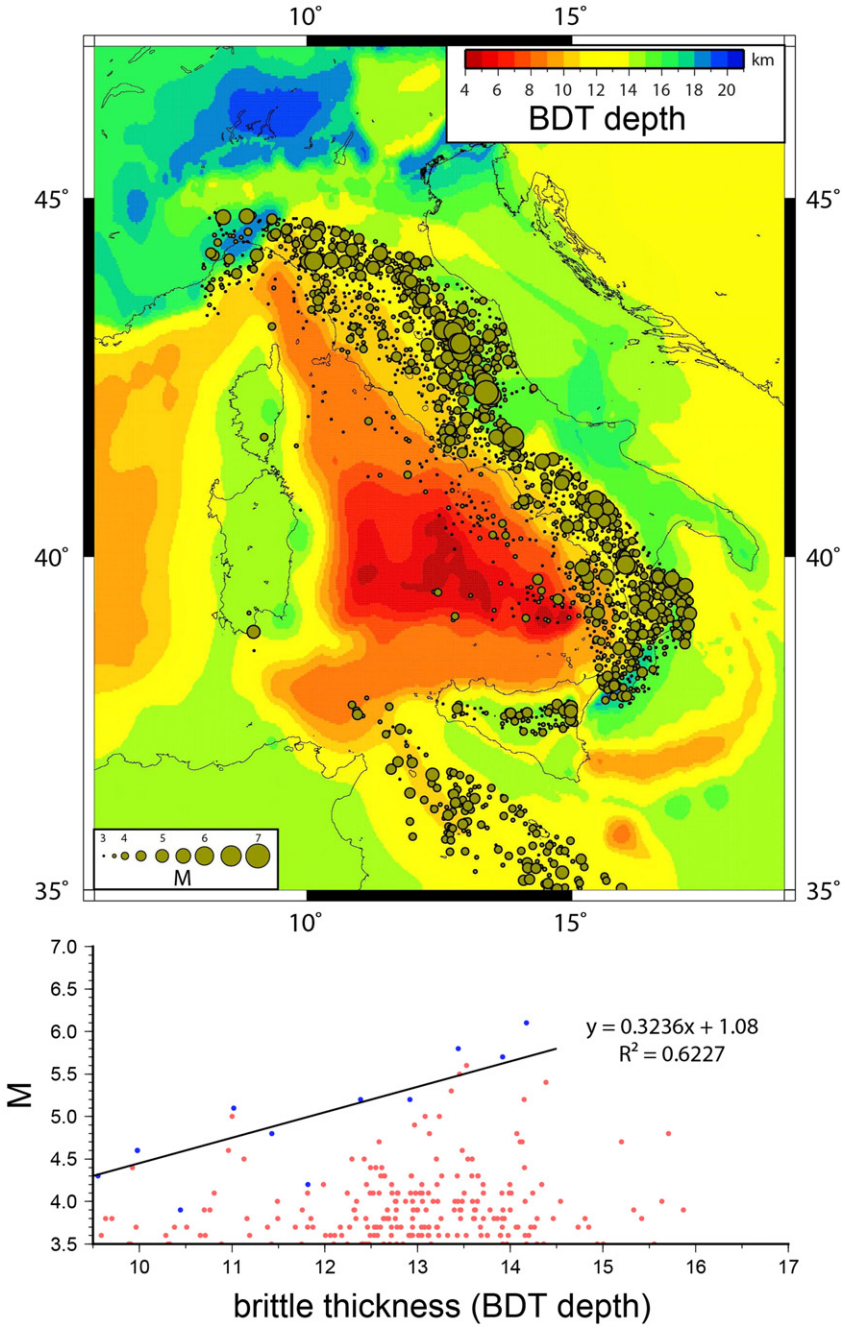

Fig. 5. Map of the brittle–ductile transition (BDT) of the Italian area and surroundings (in marine areas below seafloor), assuming a simplified two-layer crustal composition (quartz rheology for the upper crust and a diabase rheology for the lower crust) for the ductile behavior and Sibson's (1974) law for the brittle behavior, and the heat flow map of Della Vedova et al. (2001) and Petricca et al. (2013). The BDT map is modified and improved after (Barba and Doglioni, 2010; Carafa and Barba, 2011; Petricca et al., 2013). The seismicity related to normal faults increases its magnitude for increasing BDT depth. Black line in the lower panel interpolates maximum magnitudes (blue dots) observed for each bin of 0.5 km depth of the BDT. Seismic data from CSI and Iside catalogues since 1981. The BDT map is based on computations by M.M.C. Carafa.

gravity anomalies and seismic tomography (Carafa and Barba, 2011). The thermal profile for each node is then computed, at the steady state, to obtain a rough estimation of the BDT thickness.

Alternatively, we constructed detailed rheological profiles in selected localities, where good-quality data were available. The brittle layer thickness is calculated using three laws of flow: frictional faulting, dislocation creep, and Newtonian creep. This approach allowed us to compare the computed brittle (seismogenic) layer thickness and the variable Coulomb failure criterium as a function of the tectonic regime.

Last, we analyzed the depth distribution of earthquakes of the recently improved Italian National Seismic Network (http://iside.rm.ingv.it/). Earthquakes provide a direct link with the brittle (seismogenic) layer, but the data of the catalogue depend on the analyzed magnitude range and on the number and quality of past data. We systematically compared the different approaches in order to highlight similarities and to understand the differences. We found that both gross estimate and detailed rheological approach do not significantly differ in predicting the maximum thickness of the shallowmost seismogenic layer, and that the earthquake depth distribution gives comparable results in many points. The resulting analytical BDT depths do not significantly differ with those obtained by finite element models (Barba and Doglioni, 2010; Carafa & Barba 2011), having also used the same rheological parameterization (as in Barba et al., 2008; Carafa et al., 2010). On the other hand, detailed rheological profiles define, within the compressional tectonic domains, a second crustal seismogenic layer that coincides with a second mode in the earthquake depth distributions.

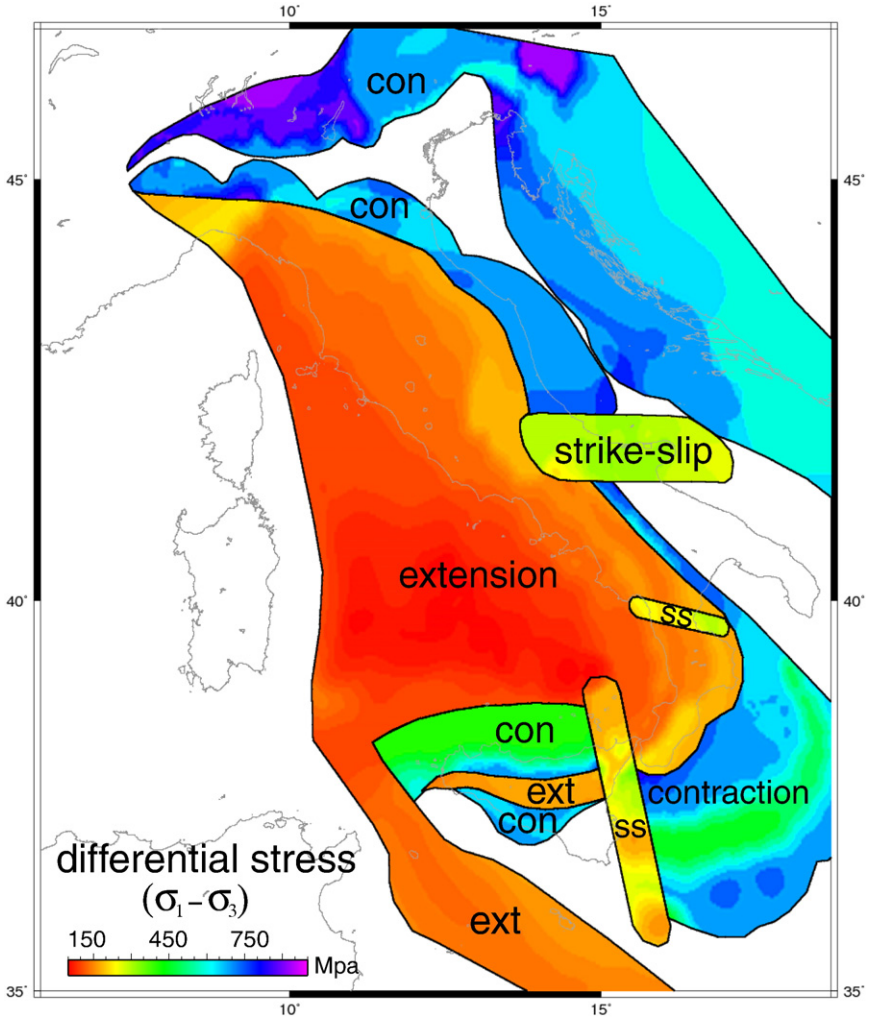

Fig. 6. Maximum differential stress in the contractional, strike–slip and extensional main tectonic settings of the Italian territory and surroundings at the BDT. The area dominated by extensional tectonics (ext) is based on regional geological data, seismicity (Fig. 2) and GPS data of Figs. 3 and 4. However, the domain characterized by regional extensional tectonics also contains secondary transfer zones or strike–slip settings, which are omitted for sake of simplicity. SS, strike–slip; con, contraction.

The map of Fig. 5 shows that the brittle layer is thicker along the axis of the Apennines where it may be 15–20 km thick, whereas moving toward the Tyrrhenian Sea rift zone, the BDT is much shallower, at 5–6 km depth beneath seafloor. Therefore, according to Fig. 4, the whole western section of the Apennines is undergoing extension, but the earthquake magnitude decreases moving from regions of deeper BDT in the east to shallower ones toward the west (Fig. 5). The stratigraphy of the region may locally contain evaporitic layers (e.g., Triassic and Messinian in age), which could favor intra-brittle crust decollement layers. However, in this work we focus only on the maximum hypothetic thickness, the related volume and the potential maximum magnitude controlled by regional brittle–ductile transition. Shallower decollements, associated with local stratigraphy, may decrease these values.

The maximum differential stress required for rock failure at the bottom of the brittle crust has been computed for the study area (Fig. 6). Following Sibson (1974), the differential stress is calculated at each node of the 1 × 1 km grid as:

$$(\sigma_1\text{-}\sigma_3) = \rho \cdot g \cdot z_{bdt} \cdot \beta \cdot (1\text{-}\lambda)$$

where $(\sigma_1 - \sigma_3)$ is the differential stress at depth z_{bdt} (i.e., the brittle–ductile transition depth, deduced from Fig. 5), ρ is the average density of the crust (2600 kg/m^3; Dziewonski and Anderson, 1981), g is the gravity acceleration, β is a numerical factor depending on the tectonic field, with values of 3, 1.2 and 0.75 for thrust, strike–slip, and normal faulting respectively (Sibson, 1974). The most uncertain parameter is λ that represents the ratio of pore-fluid pressure to lithostatic pressure. A homogeneous value of 0.4 (i.e., hydrostatic pore-fluid pressure) is assumed in our calculation. It has been shown that this value generally characterizes the crust at least down to depths of 12 km (Zoback and Townend, 2001), although significant deviations have been described associated with seismicity in the Italian area (e.g., Di Luccio et al., 2010). The study area is divided into extensional, compressional and transcurrent subdomains on the basis of seismological and paleoseismological data (e.g., Dragoni et al., 1995; Galli et al., 2008; Meletti et al., 2008), stress data (Montone et al., 2012; Carafa and Barba, 2013) regional tectonic and paleogeographic considerations (Carminati and Doglioni, 2012) and the GPS data of Figs. 3 and 4. Within these subdomains, local features could drive to deviations from the regional tectonics. For example, the subdomain characterized by extensional tectonics also contains transfer zones with active strike–slip faults (e.g., Elter et al., 2011) that are omitted for the sake of simplicity.

As expected, extensional regions show much lower differential stress with respect to the strike–slip and contractional settings. Extensional areas have horizontal σ_3 that is diminishing through time with increasing stretching, enhancing dilatancy and fracturing (Frank, 1965; Holland et al., 2011; Main et al., 2012; Schlumberger, 2013). In those volumes, if active faults creep in the ductile crust, but are locked in the brittle crust, then a dilated wedge is required to form starting at the BDT and propagating to shallower depth.

2.3. Maximum seismogenic isovolumes of Italy

Relating magnitude of earthquakes and faults by means of empirical equations is a common practice in seismological studies. Well-known relationships between fault geometry (fault area, dip, seismogenic depth, and coseismic slip, e.g., Wells and Coppersmith, 1994; Mai and Beroza, 2000; Kim and Sanderson, 2005; Leonard, 2010), fault kinematics (compressional, extensional or strike–slip regimes, e.g., Hanks and Bakun, 2002) and maximum energy releasable by a selected system are widely used. Available empirical relationships link the magnitude of an earthquake with a bi-dimensional system (the fault). However, during an earthquake a three-dimensional portion of the seismogenic crust is affected by coseismic displacement. The importance of the third dimension was already suggested by Scholz (2002) who proposed the scaling law $M_0 \sim L^2 \cdot W$, where M_0 is the scalar moment, and L and W are respectively length and width of the rupture, applicable when $W < L < 10\ W$.

As we aim to define the maximum seismic gravitational potential energy, given by a volume of rock times its density (mass), the starting point is to define the three-dimensional geometry of the system (i.e., length, depth and width; hereafter brittle volume). The maximum brittle volume depends on fault dip, brittle–ductile transition depth and rupture length (Fig. 7). In our approach the first order constraining parameter is the brittle–ductile transition depth (Fig. 5). A fixed fault dip angle of 45° or 60° (according to average values in normal faults; e.g., Sibson, 1990) is used. Assuming the BDT (at depth z_{bdt}) as the deepest tip of the activation of a seismogenic normal fault (i.e., the maximum hypocenter depth), the maximum lateral extent L of a fault reaching the Earth's surface is computed as $3 \cdot z_{bdt}$. According to Doglioni et al. (2015b), based on a review on the size of normal fault in Italy and other regions worldwide, a shape ratio $L = 3 \cdot z$ (with L and z as lateral extent of the fault and thickness of the brittle volume respectively) is consistent with the geometry of normal faults in Italy. Moreover, in several worldwide earthquakes the length of extensional faults is at most 3 times the BDT depth (e.g., Leonard, 2010; Scholz and Contreras, 1998).

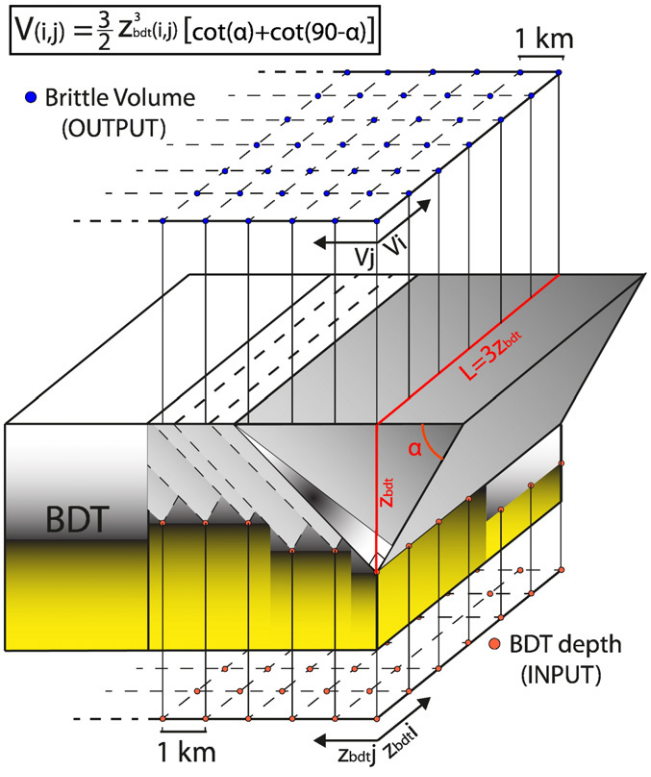

Fig. 7. Conceptual model of the maximum seismogenic volume map of Italy. The constraining parameter is the brittle–ductile transition depth (z_{bdt}) defined at each node (i, j) of a 1 × 1 km grid. Assuming that the z_{bdt} is the deepest tip of the activation of a normal fault, the corresponding seismogenic volume (V) depends on the fault dip angle (α) and the lateral extent of the fault (L). In fact, low-angle normal fault rarely generates significant magnitude earthquakes (e.g., Axen, 1999), if any. A volume shape ratio $L = 3 \cdot z$ is considered as proposed in Doglioni et al. (2015b). The volume of a triangular prism with base width corresponding to the fault and conjugated band surface projections, and delimited by a conjugated dilated wedge (here drawn only for the highlighted volume) with the same dip is given at each corresponding node of the grid (i, j). During normal faulting, the hangingwall collapses and its dimensions in terms of length (L) and width can be recognized by the distribution of the seismic cloud during the seismic swarm, and by the InSAR data detecting the subsided area (e.g., Atzori et al., 2009; Elliott et al., 2010).

The brittle volume V is computed at each node of the model (Fig. 7), using the brittle–ductile transition depth (z_{bdt}) from Fig. 5, as follows:

$$V = 3/2 \cdot z^3_{bdt} \cdot [\cot(\alpha) + \cot(90\text{-}\alpha)]$$

where α is the fault dip (e.g., 45° or 60°). This equation gives the volume of a triangular prism with base width corresponding to the fault plus the conjugated band surface projections, and delimited by the conjugated dilated wedge dipping as portrayed in Fig. 1. Values up to about $2 \cdot 10^4$ km^3 are obtained in areas characterized by thick brittle layers (Fig. 8) in extensional regime (e.g., Calabria, Southern Italy). The inferred dilated wedge may eventually evolve into a conjugated normal fault to form a graben. Fig. 8 shows the results of a preliminary exercise assuming 45° and 60° dip for the normal fault, consistent with the average 45° dip angle of the fault activated during the 2009 L'Aquila M_w 6.3 earthquake (Chiarabba et al., 2009), or the 60° dip of the 1980 Irpinia M_w 6.9 earthquake (Bernard and Zollo, 1989). The model should be tested in the future assuming different fault dip angles and including other parameters such as friction, strain rate, etc.

Using the equations of Doglioni et al. (2015a), the potential seismic energy can be quantified from the involved seismogenic volumes. Then applying the relationship reported in Choy and Boatwright (1995), we obtain the maximum possible magnitude (M). The potential energy really available to generate an earthquake of magnitude M is given by the potential energy reduced by a fraction due to friction: the potential residual energy RU is then

$$RU = mg \cdot (1\text{-}\mu \cdot \cos\alpha) \cdot u_s = \rho V g \cdot (1\text{-}\mu \cdot \cos\alpha) \cdot u_s$$

where $m = \rho V$ is the mass of a volume V having density ρ (the average value for continental crust is 2600 kg/m^3 Dziewonski and Anderson, 1981); μ is the fault friction coefficient (e.g., 0.6 according to Byerlee, 1978) and u_s the average coseismic slip.

Then, the maximum possible magnitude M computed from Choy and Boatwright (1995) is

$$M = 2/3 \cdot \log(RU \cdot r_c) - 3.2$$

where r_c is the seismic radiation coefficient (Aki and Richards, 1980), which is here assumed to be 0.03 (Choy and Boatwright, 1995).

We have mapped the value of M obtained with the previous relationship on 1 × 1 km regular grid. The maximum involved volume (bounded by the fault and by the antithetic dilated band) can be computed, as done in Fig. 8 for the Italian area, assuming a fault dip of 45° and 60°. Larger volumes imply larger displacement and in particular larger gravitational potential energy involved in potential earthquakes. The resulting magnitudes are shown in Fig. 9 only for regions of the study area characterized by extensional tectonic regime. In our calculation, average coseismic slip (u_s) increases with volume from 5 to 200 cm, consistently with the observed correlation between slip and magnitudes (Fig. 9 lower panel) observed in seismological data (e.g., Leonard, 2010). To support the M_w increase with fault dip, we compared the magnitude with the dip of faults for extensional earthquakes with $M_w > 4.5$ available in the instrumental record (gCMT and rCMT compilations; time span 1976–2011), plus well constrained parameters from historical events. Instrumental data selection follows

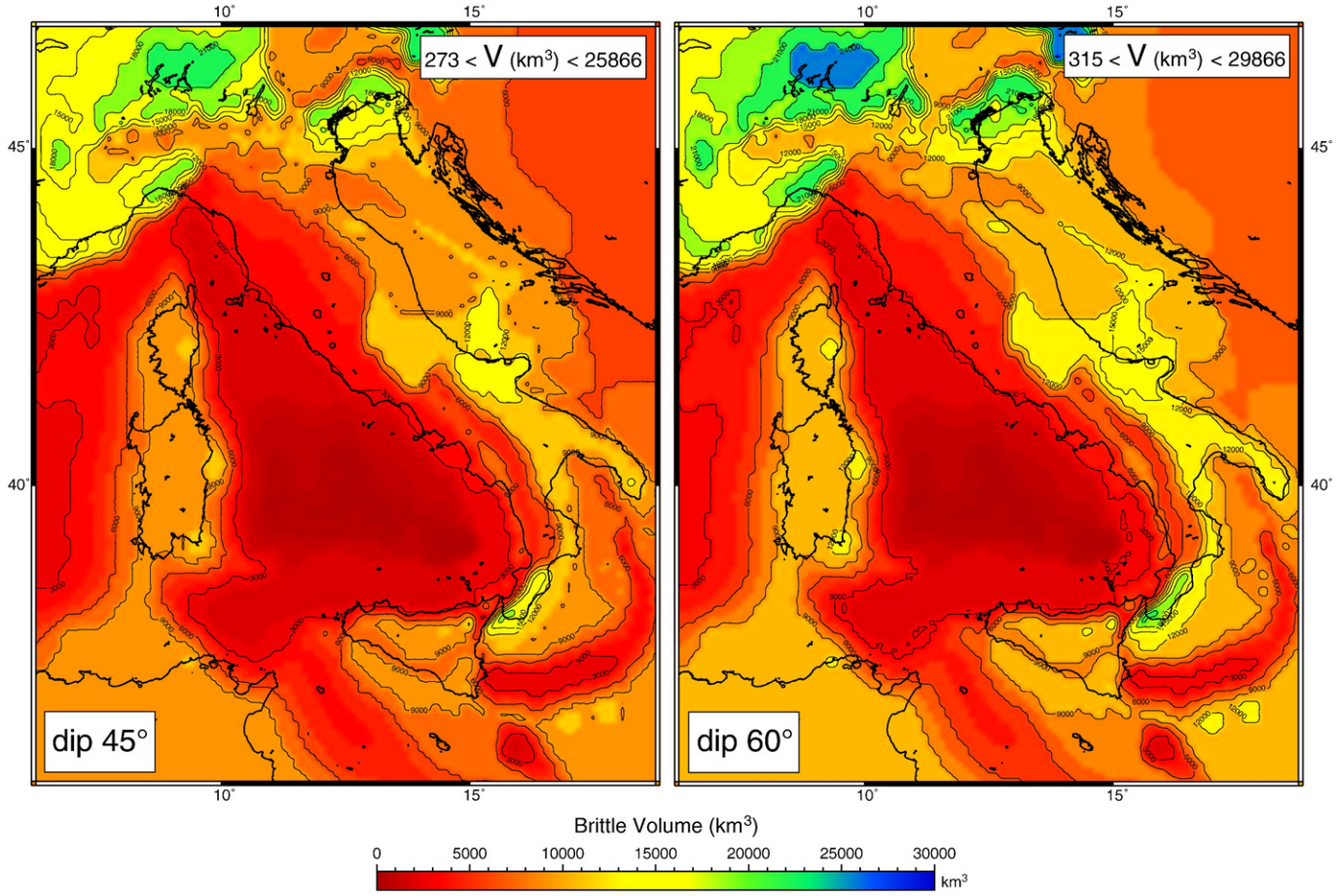

Fig. 8. Assuming a mean maximum normal fault length three times the hypocenter depth, and a triangular shape of the hangingwall above a 45° (left) and 60° (right) dipping normal fault and the conjugate dilated band, the deeper the BDT, the larger the volume involved. These maps of the Italian territory and surroundings represent the upper crustal brittle isovolumes that can be mobilized by a hypothetical normal fault. Increasing the fault dip should also correspond to an increase of the vertical component of the coseismic slip.

the scheme proposed by Kagan (2005), and is based on plunges of the axes from the focal mechanisms. This reduced the initial 494 records to 86 normal events. Once we classified a normal earthquake, its preferred rupture plane was selected on regional tectonic considerations. As Italian earthquakes with large magnitudes have recurrence times >300 years, greater than the time span of instrumental records <40 years, historical events integration is required for completeness. In this case, the selection was made on the basis of geologic evidences, with magnitude and fault dip parameters extracted from the DISS database (Basili et al., 2008). This allowed us to include 7 more normal events in statistical analysis.

When considering regions under tension in Italy, the maximum magnitude is predicted along the Apennines axis, where the brittle layer is thicker (Fig. 5) and the normal faults are steeper (Fig. 10).

According to the model presented here, the maximum potential magnitude computed in the extensional areas of Italy is around 7.5, depending on the assumed parameters. A sensitivity analysis performed using different dip angles for the faults (30° to 60°), varying the average coseismic slips on fault (20 to 80 cm) and fault friction coefficient (0.4 to 0.8), points out the stability of the proposed model to define the maximum magnitude (variations in the range of ±0.2; Fig. 11).

3. Normal faulting in peninsular Italy

A schematic cross-section of the central-northern Apennines (Fig. 12) illustrates the subduction system characterized by a NE-ward retreating slab and the related frontal accretionary prism to the east and the backarc extension to the west. In the extensional domain of the Apennines, major normal faults cut through the brittle upper crust and the ductile lower crust (Bigi et al., 2002). Major NE-dipping normal faults associated with the subduction hinge retreat have conjugate SW-dipping normal faults that may branch at different depths. Examples are the NE-dipping low-angle (15–30°) Alto Tiberina fault and its conjugated shallower and steeper SW-dipping normal faults responsible for the 1997–1998 Umbria–Marche seismic sequence (e.g., Mirabella et al., 2011), or the NE-dipping steeper (50–60°) and deeper Irpinia fault responsible for the M 6.9, 1980 Irpinia earthquake, having a deeper and steeper conjugate normal fault (Pingue and De Natale, 1993). Therefore, regional NE-dipping normal fault may steadily creep and show low-magnitude seismicity (e.g., the Alto Tiberina Fault), or alternatively be locked and responsible for higher magnitude seismicity (Irpinia Fault). Steeper normal faults are usually associated with higher friction rocks and events of larger magnitude (Doglioni et al., 2015b).

It has been shown in the previous section that, regardless where are located the seismogenic faults, the maximum expected volume and the maximum potential magnitude can be calculated. This is particularly important for Italy, where most of the extensional faults that produced major earthquakes in the last 35 years were blind and in some cases unknown to seismologists and geologists. However more discussion on two points is needed.

It has been discussed that a deeper branching between main and conjugate faults is associated with a bigger volume (Figs. 1 and 7). Therefore, when the hypocenter of an earthquake is shallower than

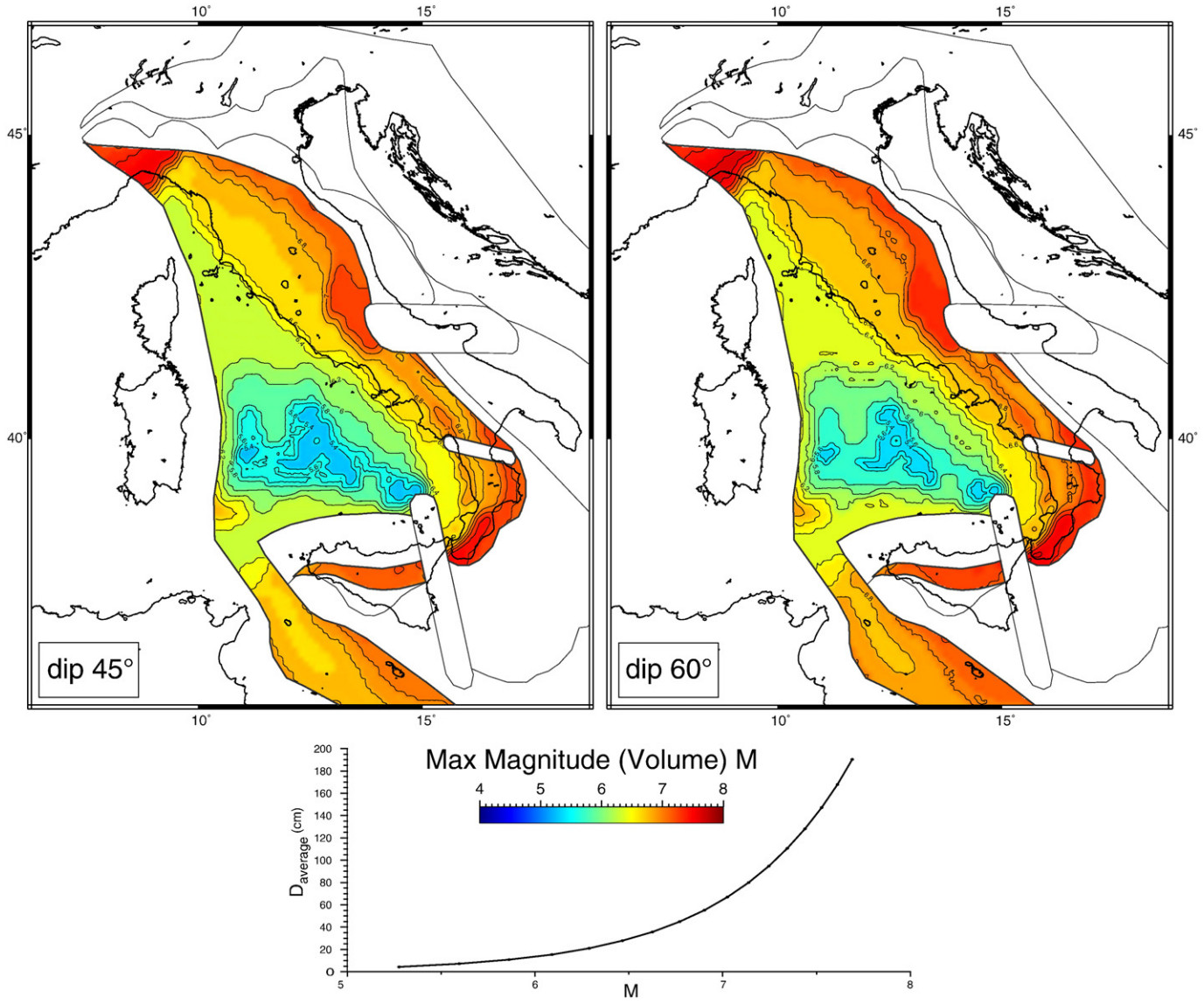

Fig. 9. The maps show the maximum magnitude (M) expected by gravitational collapse along normal faults in the Italian area and surroundings undergoing extensional tectonics, assuming a slip (D) increasing with magnitude as reported in the lower diagram. The values are inferred assuming the collapse of the volumes computed in the previous figure (45° left and 60° right). It is hypothesized a constant static friction, and normal fault planes activated during an earthquake seem to have in average a mean maximum length three times the depth of the hypocenter. Normal fault earthquakes have their maximum magnitude close to the brittle–ductile transition (BDT), which is deeper where the surface heat flow is lower. The deeper the BDT, the larger the volume and the higher will result the graviquake magnitude. These maps of the extensional areas affecting the central Mediterranean, are only a preliminary attempt to relate brittle volumes and maximum potential magnitude, if active normal faults are present.

the BDT, the magnitude of an earthquake will be smaller than the maximum expected magnitude. For example, the M_w 6.3 L'Aquila April 6, 2009 earthquake has been smaller than the maximum potential earthquake for that area because the hypocenter was possibly 5–8 km shallower than the BDT (Fig. 12). A second point to be emphasized is that the maximum expected magnitude map does not necessarily mean that (large) extensional earthquakes will occur where large magnitudes are indicated. For example, the thick brittle crust in Sardinia results in very high (up to 6.8) maximum expected magnitudes. Sardinia has been subject to E–W stretching in Oligocene–Miocene times and NE–SW stretching in the Campidano graben in Pliocene–recent times (Casula et al., 2001). However, the GPS velocity pattern evidences insignificant deformation rate. This means that the potential to generate large earthquakes in this region most likely will not be activated. However, it cannot be excluded that large earthquakes could occur with very long recurrence times. The consistency of the importance of the involved volume is supported for example by the observation that thin brittle-elastic crust generates low-magnitude events, even in case of fast spreading rates as along the East Pacific Rise (Shen, 2002).

Finally a consequence on paleoseismological studies is highlighted. Morellato et al. (2003) measured the average spacing among normal faults of about 4–6 km both in the Apennines and in several other stretching regions worldwide. However, when an earthquake occurs, say, at 10 km depth and the branching between main and conjugate faults is located at the same depth, the conjugate boundary or fault will intersect the Earth's surface at a distance of about 10–15 km (depending on the fault dip) from the slipping fault plane. Since the average spacing of normal faults is shorter, it means that several faults are passively shifted downward within the falling volume of the hangingwall during the coseismic stage. Therefore, accurate paleoseismological studies along a fault plane (e.g., Galli and Peronace, 2014; Galli et al., 2015) are able to constrain the tectonic history and the seismic cycle of that single fault but not of the few kilometers of adjacent faults and the surrounding region. This also means that rupture

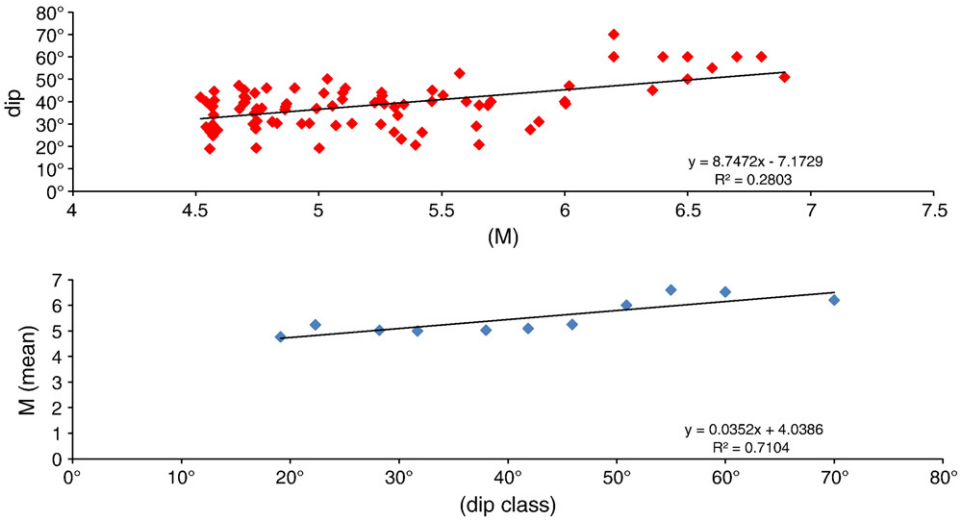

Fig. 10. Panel above, dip vs. M_w of normal fault earthquakes with $M_w > 4.5$ for the Italian peninsula (1976–2011, gCMT and rCMT, plus 7 other well constrained historical events). The correlation coefficient of 0.53 obtained from fitting 93 pairs of observations ensures its statistical significance. Panel below, for the same catalogs statistical relationship between M_w and fault dip angles binned by classes (every 5°), again supporting the M_w increase with fault dip with a significant correlation of 0.84 (Fisher and Yates, 1963). Slightly modified after Doglioni et al., 2015b.

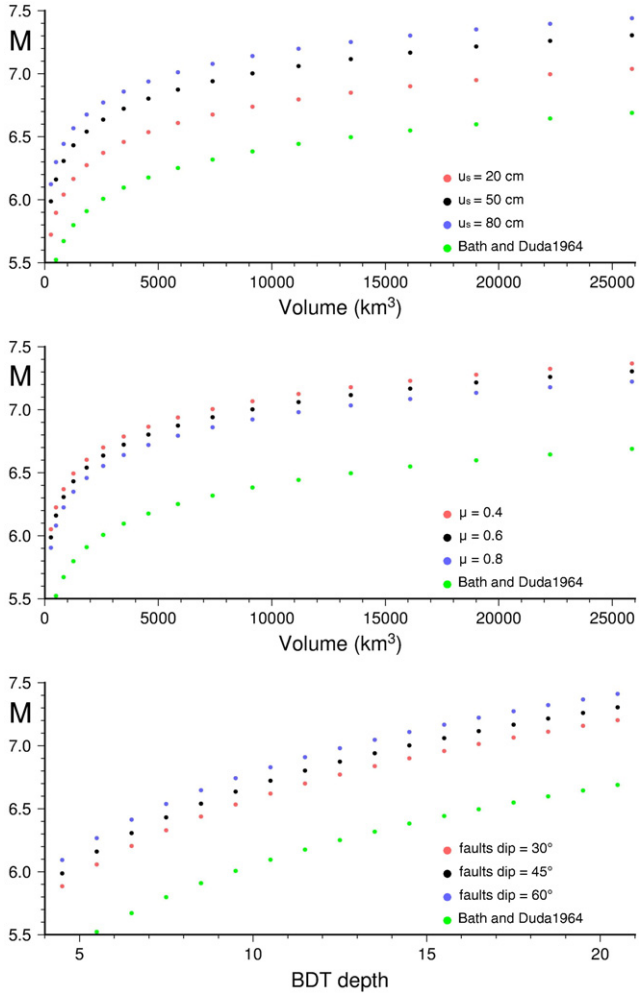

Fig. 11. Variation of magnitude as a function of the normal fault slip, friction and volume, according to the parameters used in the text. A comparison with the magnitudes computed according the Bath and Duda (1964) relationship is also shown.

occurs randomly, moving laterally both along dip and strike from one fault to the other and that probabilistic time recurrence studies may miss several seismic events in adjacent fault planes.

Riguzzi et al. (2012) have shown that the higher magnitude earthquakes occur in areas where the strain rate is lower, i.e., in active tectonic settings, the locked faults accumulate larger energy. The higher strain rates may rather be related either to post-event relaxation or to mean lower fictional parameters in the upper crust of peninsular Italy, and they may decrease the maximum expected magnitude computed assuming the gravitational potential energy.

4. Discussion

Earthquakes with magnitude similar to the maximum obtained by our calculation (M 7.5) occur worldwide in extensional environments, independently of the values reached by geodetic strain rates. Examples are areas with very low extension rates (1–2 mm/year) such as the 1811–1812, M 7–7.5 (8?) New Madrid earthquakes in central North America (Calais et al., 2005 and references therein), and in areas characterized by higher rates (4–5 mm/year) such as along the East African Rift (1990, M 7.1 north of Alberta Lake; 2006, M 7 West Mozambique; Yang and Chen, 2010) and the Baikal rift (2008 M 6.3; Sloan et al., 2011). This implies that the earthquake magnitude is primarily controlled by the involved volume, whereas the extension rate rather appears to control the recurrence time of the earthquakes, being the recurrence more frequent for faster extension.

Normal faults display a range of potential dip angles (Sibson, 1990). Large earthquakes do not occur along low-dip normal faults (Jackson and White, 1989). The dip of the normal faults depends on the friction of the involved rocks. The higher the friction, the steeper is the fault. In the graviquake model (Doglioni et al., 2015b), for a fixed amount of extension, steeper faults will be characterized by larger vertical components of fault slip. Therefore we should expect higher magnitude for steeper faults. We compared the magnitude of the Italian extensional earthquakes with the dip of the faults and it results, as expected, that steeper faults are characterized by earthquakes with lower frequency and larger magnitude (Fig. 10). The higher the slip (i.e., the lower the friction), or the fault dip, the larger will result the magnitude (Fig. 11). Our analysis is clearly biased by the short time span (35 years) of the

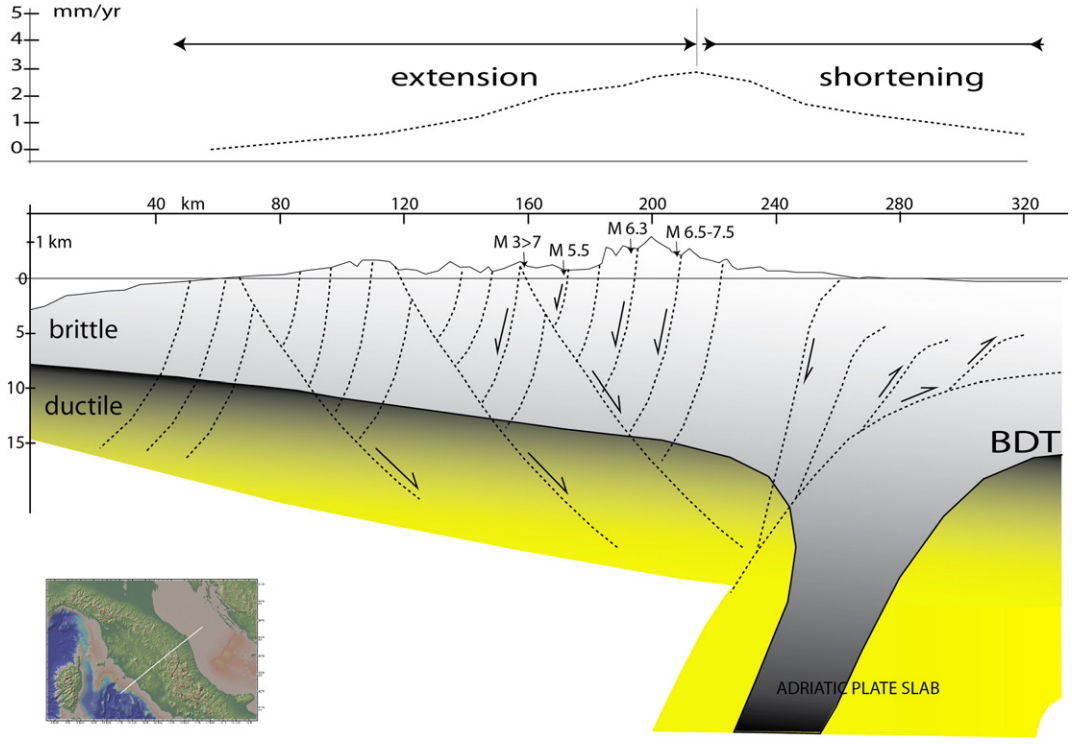

Fig. 12. Schematic cross-section of the central Apennines. NE-dipping faults associated with the subduction hinge retreat have conjugate SW-dipping normal faults. The shallower the branch line of the conjugate fault, the smaller the volume and the related earthquake magnitude. Moreover low-angle NE-dipping normal faults (e.g., the Alto Tiberina fault, Chiaraluce et al., 2007) may creep and release less energy due to the lower friction. When adopting the gravitational model in which the earthquake along a normal fault is generated by the collapse of the hangingwall closing the crustal volume previously stretched during the interseismic period, it may happen that only a shallow part of the hangingwall collapses (Fig. 1). In this case the magnitude will be smaller than if the entire brittle layer above the brittle–ductile transition collapses. This may be the case for the L'Aquila 2009 M_w 6.3 event, which had the hypocenter at about 9–10 km, whereas the BDT is at 15–18 km. If the black brittle segment was activated, an M around 7 could have occurred. This tectonic model does not apply to Sicily, where contraction occurs also in the Tyrrhenian side of the upper plate (Figs. 4 and 6).

seismic catalogue (1976–2011). In fact, normal faults may have recurrence time of even 600 years (Riguzzi et al., 2013) and the higher magnitude events recorded in the analyzed time frame are certainly incomplete for determining a reliable Gutenberg–Richter distribution. Nevertheless, the earthquakes having M > 4.5 indicate a positive correlation between fault dip and magnitude (Fig. 10).

The general assumption in seismology is that earthquake magnitude depends on the rupture area and coseismic displacement. This is empirically demonstrated and possibly still valid. However, we have shown that the rupture area and its displacement are consequence and constrained by the volume in which a given potential energy is accumulated, either gravitational or elastic. On the basis of the BDT depth (Fig. 5), we computed the maximum volume (Fig. 8) expected to be mobilized in areas of peninsular Italy where crustal extension is demonstrated by geology, seismicity (Fig. 2) and GPS velocity field (Fig. 4). The volume is transformed into mass and available gravitation potential energy (Fig. 9). In fact, normal faults rupture initiates at depth where the lithostatic load is maximum, and then propagates upward (Carminati et al., 2004). The results show that gravitational energy can generate earthquakes of magnitude comparable with the observed historic seismicity. The maximum expected magnitude increases both with the volume involved (Fig. 9) and with the dip of the fault (Fig. 10) as suggested in Doglioni et al. (2011; 2015b). The magnitudes calculated from the volume defined by the aftershocks (Bath and Duda, 1964) systematically underestimate our magnitudes (Fig. 11). One possible explanation is that due to seismic network capability not all the aftershocks are correctly positioned or even recorded those below the completeness threshold, and for sure in 1964 only the largest were collected. However, the area undergoing extension is subject to i) lateral variation of lithologies, rheological parameters (Pauselli et al., 2010); ii) volumetric variations of the pore-fluid pressure (e.g., Di Luccio et al., 2010; Doglioni et al., 2014); iii) transfer zones and strike–slip faults along inherited lithological changes of facies and thickness that disturb the cylindricity of normal faults, inhibiting lateral propagation of the fault rupture and involvement of large related volume; iv) lateral and along strike migration of the rupture (e.g., Boncio et al., 2004), possibly preventing probabilistic studies of seismic recurrence along a single fault (Panza et al., 2012). Such parameters may further deeply vary the friction and the differential stress threshold for energy dissipation and earthquake nucleation. All these issues generally tend to decrease the maximum earthquake magnitude expected from the simple volumetric approach described in this research.

Normal fault-related earthquakes show a higher *b* value of the Gutenberg–Richter law (Schorlemmer et al., 2005). This implies that such earthquakes have lower magnitude with respect to strike–slip and thrust-related earthquakes. This is consistent with the smaller maximum volumes involved by normal faulting earthquakes with respect to the other tectonic settings (Doglioni et al., 2015b).

5. Conclusions

In this article we tested in the natural laboratory of Italy the hypothesis that crustal normal fault earthquakes (graviquakes) are essentially dominated by the dissipation of gravitational potential energy, which is accumulated during the interseismic period due to the pressure gradient forming at the BDT for the differential behavior of the constantly shearing ductile lower crust, and the brittle stick–slip upper crust (Fig. 1). Since gravitational collapse delivers energy far greater than that dissipated by the earthquakes, the hangingwall collapse can certainly explain the earthquake magnitude, being the extra energy dissipated by shear heating and

fracturing (Doglioni et al., 2015b; Fulton and Rathbun, 2011; Kanamori and Rivera, 2006). The fall of the hangingwall of the normal fault is allowed by the presence of a dilated inclined wedge generated from the BDT upward that can absorb the volume decrement during the collapse (Fig. 1). This wedge is kinematically and mechanically required by the strain partitioning between the brittle upper crust and the ductile lower crust. Since the normal fault hangingwall suddenly subsides during the coseismic stage, there must be a crustal dilated volume at depth that can allow this fall. Based on this model, the shallower the lower tip of the normal fault, the smaller is the related volume, displacement and earthquake (Figs. 1 and 11). The maximum volume potentially involved, and consequently the earthquake magnitude, is determined by the depth of the BDT. The model presented here is a preliminary demonstration that earthquakes have different mechanisms as a function of the tectonic style. Moreover we show that the volume surrounding the fault is the real accumulator of potential energy rather than the fault itself. In extensional tectonic settings gravitational energy dominates, whereas elastic energy is the primary source for contractional tectonic environments. Therefore, fault evolution and precursors may be different for each one of the three main geodynamic settings (extension, contraction and strike–slip).

Acknowledgments

Thanks for fruitful discussions to Andrea Billi, Cristiano Collettini, Marco Cuffaro, Miriam Lombardo, Chris Scholz, Davide Scrocca, Giancarlo Ventura, Fabio Trippetta and Natalia Zamora. Constructive reviews by Emilio Casciello and François Roure were greatly appreciated. Funding by PRIN2010/11 (Project 20107ESMX9 “Crisi e ripresa di sistemi carbonatici e potenziale per la formazione di reservoir: i ruoli di clima, tettonica e magmatismo” and project 2010PMKZX7_004 “La subduzione e l'esumazione di litosfera continentale: i suoi effetti sulla struttura degli orogeni, sull'ambiente e sul clima”) are acknowledged by Eugenio Carminati and Carlo Doglioni. Roberto Devoti and Grazia Pietrantonio contributed to the GPS velocity estimation. The BDT map of Fig. 5 has been obtained with data and computations provided by Michele M.C. Carafa. Most figures were produced using the GMT software.

References

Aki, K., Richards, P., 1980. Quantitative Seismology. W.H. Freeman, New York (932 pp.).
Atzori, S., Hunstad, I., Chini, M., Salvi, S., Tolomei, C., Bignami, C., Stramondo, S., Trasatti, E., Antonioli, A., Boschi, E., 2009. Finite fault inversion of DInSAR coseismic displacement of the 2009 L'Aquila earthquake (central Italy). Geophys. Res. Lett. 36, L15305. http://dx.doi.org/10.1029/2009GL039293.
Axen, G.J., 1999. Low-angle normal fault earthquakes and triggering. Geophys. Res. Lett. 26, 3693–3696. http://dx.doi.org/10.1029/1999GL005405.
Barba, S., Carafa, M.C., Boschi, E., 2008. Experimental evidence for mantle drag in the Mediterranean. Geophys. Res. Lett. 35, L06302. http://dx.doi.org/10.1029/2008GL033281.
Barba, S., Doglioni, C., 2010. Project S1: Analysis of the seismic potential in Italy for the evaluation of the seismic hazard. Istituto Nazionale di Geofisica e Vulcanologia - Dipartimento Protezione Civile, Agreement INGV-DPC 2007-2009 http://www.earth-prints.org/handle/2122/7958.
Basili, R., Valensise, G., Vannoli, P., Burrato, P., Fracassi, U., Mariano, S., Tiberti, M.M., Boschi, E., 2008. The Database of Individual Seismogenic Sources (DISS), version 3: summarizing 20 years of research on Italy's earthquake geology. Tectonophysics 453, 20–43. http://dx.doi.org/10.1016/j.tecto.2007.04.014.
Basili, R., Kastelic, V., Demircioglu, M.B., Garcia, Moreno, Nemser, E.S., Petricca, P., Sboras, S.P., Besana-Ostman, G.M., Cabral, J., Camelbeeck, T., Caputo, R., Danciu, L., Domac, H., Fonseca, J., García-Mayordomo, J., Giardini, D., Glavatovic, B., Gulen, L., Ince, Y., Pavlides, S., Sesetyan, K., Tarabusi, G., Tiberti, M.M., Utkucu, M., Valensise, G., Vanneste, K., Vilanova, S., Wössner, J., 2013. The European Database of Seismogenic Faults (EDSF) compiled in the framework of the Project SHARE. http://dx.doi.org/10.6092/INGV.IT-SHARE-EDSF http://diss.rm.ingv.it/share-edsf/.
Bath, M., Duda, S.J., 1964. Earthquake volume, fault plane area, seismic energy, strain, deformation and related quantities. Ann. Geofis. 17, 353–368.
Bernard, P., Zollo, A., 1989. The Irpinia (Italy) 1980 earthquake: detailed analysis of a complex normal faulting. J. Geophys. Res. 94 (B2), 1631–1647.
Beutler, G., et al., 2007. In: Dach, R., Hugentobler, U., Fridez, P., Meindl, M. (Eds.), Bernese GPS Software Version 5.0. Astronomical Institute, University of Bern.
Bigi, S., Doglioni, C., Mariotti, G., 2002. Thrust vs normal fault decollements in the central Apennines. Boll. Soc. Geol. Ital. Spec. 1, 161–166.
Boncio, P., Lavecchia, G., Pace, B., 2004. Defining a model of 3D seismogenic sources for seismic hazard assessment applications: the case of central Apennines (Italy). J. Seismol. 8, 407–425.
Byerlee, J., 1978. Friction of rocks. Pure Appl. Geophys. 116 (4-5), 615–626.
Calais, E., Mattioli, G., DeMets, C., Nocquet, J.-M., Stein, S., Newman, A., Rydelek, P., 2005. Tectonic strain in plate interiors? Nature 438. http://dx.doi.org/10.1038/nature04428.
Carafa, M.M.C., Barba, S., 2011. Determining rheology from deformation data: the case of central Italy. Tectonics 30, TC2003. http://dx.doi.org/10.1029/2010TC002680.
Carafa, M.M.C., Barba, S., Conti, L., Megna, A., 2010. Deliverable D5.03.04, Model-predicted strain rate map. In: Barba, S., Doglioni, C. (Eds.), Project S1: Analysis of the seismic potential in Italy for the evaluation of the seismic hazard ftp://ftp.ingv.it/pro/dpcs1_dati/Relazioni_2anno_temp/5.03_Megna/.
Carminati, E., Doglioni, C., 2012. Alps vs. Apennines: the paradigm of a tectonically asymmetric Earth. Earth Sci. Rev. 112, 67–96. http://dx.doi.org/10.1016/ j.earscirev.2012.02.004.
Carafa, M.M.C., Barba, S., 2013. The stress field in Europe: optimal orientations with confidence limits. Geophys. J. Int. 193, 531–548.
Carminati, E., Doglioni, C., Barba, S., 2004. Reverse migration of seismicity on thrusts and normal faults. Earth Sci. Rev. 65, 195–222.
Carminati, E., Lustrino, M., Doglioni, C., 2012. Geodynamic evolution of the central and western Mediterranean: tectonics vs. igneous petrology constraints. Tectonophysics 579, 173–192. http://dx.doi.org/10.1016/j.tecto.2012.01.026.
Casula, G., Cherchi, A., Montadert, L., Murru, M., Sarria, E., 2001. The Cenozoic graben system of Sardinia (Italy): geodynamic evolution from new seismic and field data. Mar. Pet. Geol. 18, 863–888.
Chiarabba, C., et al., 2009. The 2009 L'Aquila (central Italy) MW 6.3 earthquake: main shock and aftershocks. Geophys. Res. Lett. 36, L18308. http://dx.doi.org/10.1029/2009GL039627.
Chiaraluce, L., Chiarabba, C., Collettini, C., Piccinini, D., Cocco, M., 2007. Architecture and mechanics of an active low-angle normal fault: Alto Tiberina Fault, northern Apennines, Italy. J. Geophys. Res. 112, B10310. http://dx.doi.org/10.1029/2007JB005015.
Choy, G.L., Boatwright, J.L., 1995. Global patterns of radiated seismic energy and apparent stress. J. Geophys. Res. 100 (B9), 18205–18228. http://dx.doi.org/10.1029/95JB01969.
Cooke, M.L., Murphy, S., 2004. Assessing the work budget and efficiency of fault systems using mechanical models. J. Geophys. Res. 109, B10408. http://dx.doi.org/10.1029/2004JB002968.
Dahlen, F.A., 1977. The balance of energy in earthquake faulting. Geophys. J. R. Astron. Soc. 48, 239–261.
Della Vedova, B., Bellani, S., Pellis, G., Squarci, P., 2001. Deep temperatures and surface heat flow density distribution. In: Vai, G.B., Martini, P. (Eds.), Anatomy of an Orogen: The Apennines and Adjacent Mediterranean Basins. Kluwer Academic Publishers, Dordrecht, Netherlands, pp. 65–76.
Dempsey, D., Ellis, S., Archer, R., Rowland, J., 2012. Energetics of normal earthquakes on dip-slip faults. Geology 40, 279–282.
Devoti, R., Riguzzi, F., Cuffaro, M., Doglioni, C., 2008. New GPS constraints on the kinematics of the Apennine subduction. Earth Planet. Sci. Lett. 273 (1–2), 163–174.
Devoti, R., Pietrantonio, G., Pisani, A.R., Riguzzi, F., Serpelloni, E., 2010. Present day kinematics of Italy. In: Beltrando, M., Peccerillo, A., Mattei, M., Conticelli, S., Doglioni, C. (Eds.), J. Virtual Explorer 36 (2). http://dx.doi.org/10.3809/jvirtex.2009.00237.
Devoti, R., Esposito, A., Pietrantonio, G., Pisani, A.R., Riguzzi, F., 2011. Evidence of large scale deformation patterns from GPS data in the Italian subduction boundary. Earth Planet. Sci. Lett. 311, 230–241.
Devoti, R., Pietrantonio, G., Pisani, A.R., Riguzzi, F., 2014. GNSS networks for geodynamics in Italy. Fisica de la Tierra 26. Universidad Complutense de Madrid, pp. 11–24 (http://revistas.ucm.es/index.php/FITE/article/view/46968).
Devoti, R., Pietrantonio, G., Pisani, A.R., Riguzzi, F., 2015. Permanent GPS networks in Italy: analysis of time series noise. Int. Ass. Geodesy Symp. 142. Springer, pp. 1–8. http://dx.doi.org/10.1007/1345_2015_11.
Di Luccio, F., Ventura, G., Di Giovambattista, R., Piscini, A., Cinti, F.R., 2010. Normal faults and thrusts re-activated by deep fluids: the 6 April 2009 Mw 6.3 L'Aquila earthquake, central Italy. J. Geophys. Res. 115 (B06315), 15. http://dx.doi.org/10.1029/2009JB007190.
Doglioni, C., Barba, S., Carminati, E., Riguzzi, F., 2011. Role of the brittle–ductile transition on fault activation. Phys. Earth Planet. Int. 184, 160–171. http://dx.doi.org/10.1016/j.pepi.2010.11.005.
Doglioni, C., Barba, S., Carminati, E., Riguzzi, F., 2014. Fault on–off versus coseismic fluids reaction. Geosci. Front. 5, 767–780. http://dx.doi.org/10.1016/j.gsf.2013.08.004.
Doglioni, C., Barba, S., Carminati, E., Riguzzi, F., 2015a. Fault on–off versus strain rate and earthquakes energy. Geosci. Front. 6, 265–276. http://dx.doi.org/10.1016/j.gsf.2013.12.007.
Doglioni, C., Carminati, E., Petricca, P., Riguzzi, F., 2015b. Normal fault earthquakes or graviquakes. Sci. Rep. 5:12110, 1–12. http://dx.doi.org/10.1038/srep12110.
Dragoni, M., Doglioni, C., Mongelli, F., Zito, G., 1995. Evaluation of stresses in two geodinamically different areas: stable foreland and extensional back-arc. PAGEOPH 146 (2), 319–341.
Dziewonski, A.M., Anderson, D.L., 1981. Preliminary reference Earth model. Phys. Earth Planet. Inter. 25 (4), 297–356.
Elliott, J.R., Walters, R.J., England, P.C., Jackson, J.A., Li, Z., Parsons, B., 2010. Extension on the Tibetan plateau: recent normal faulting measured by InSAR and body wave seismology. Geophys. J. Int. 183 (2), 503–535. http://dx.doi.org/10.1111/j.1365-246X.2010.04754.x.
Elter, F.M., Elter, P., Eva, C., Eva, E., Kraus, R.K., Padovano, M., Solarino, S., 2011. Strike–slip geometry inferred from the seismicity of the Northern-Central Apennines (Italy). J. Geodyn. 52, 379–388.

Fisher, R.A., Yates, F., 1963. Statistical Tables for Biological, Agricultural and Medical Research. Oliver and Boyd, L.t.d, Edinburgh.
Frank, F.C., 1965. On dilatancy in relation to seismic sources. Rev. Geophys. 3, 485–503.
Fulton, P.M., Rathbun, A.P., 2011. Experimental constraints on energy partitioning during stick–slip and stable sliding within analog fault gouge. Earth Planet. Sci. Lett. 308 (1), 185–192.
Galli, P., Peronace, E., 2014. New paleoseismic data from the Irpinia Fault. A different seismogenic perspective for southern Apennines (Italy). Earth Sci. Rev. 136, 175–201. http://dx.doi.org/10.1016/j.earscirev.2014.05.013.
Galli, P., Galadini, F., Pantosti, D., 2008. Twenty years of paleoseismology in Italy. Earth Sci. Rev. 88, 89–117.
Galli, P., Giaccio, B., Peronace, E., Messina, P., 2015. Holocene paleoearthquakes and Early–Late Pleistocene slip-rate on the Sulmona Fault (Central Apennines, Italy). Bull. Seismol. Soc. Am. 105, 1. http://dx.doi.org/10.1785/0120140029.
Hanks, T.C., Bakun, W.H., 2002. A bilinear source-scaling model for M–log A observations of continental earthquakes. Bull. Seismol. Soc. Am. 92, 1841–1846.
Holland, M., van Gent, H., Bazalgette, L., Yassir, N., Hoogerduijn Strating, E.H., Urai, J.L., 2011. Evolution of dilatant fracture networks in a normal fault—evidence from 4D model experiments. Earth Planet. Sci. Lett. 304, 399–406. http://dx.doi.org/10.1016/j.epsl.2011.02.017.
Hreinsdóttir, S., Bennett, R.A., 2009. Active aseismic creep on the Alto Tiberina low-angle. Geology 37 (8), 683–686. http://dx.doi.org/10.1130/G30194A.
Jackson, J.A., White, N.J., 1989. Normal faulting in the upper continental crust: observations from regions of active extension. J. Struct. Geol. 11, 15–36.
Kagan, Y.Y., 2005. Double-couple earthquake focal mechanism: random rotation and display. Geophys. J. Int. 163, 1065–1072. http://dx.doi.org/10.1111/j.1365-246X.2005.02781.x.
Kanamori, H., Rivera, L., 2006. Energy partitioning during an earthquake. In: Abercrombie, R., McGarr, A., Di Toro, G., Kanamori, H. (Eds.), Earthquakes: Radiated Energy and the Physics of Faulting. AGU, Washington, D. C http://dx.doi.org/10.1029/170GM03.
Kim, Y.-S., Sanderson, D.J., 2005. The relationship between displacement and length of faults: a review. Earth Sci. Rev. 68, 317–334. http://dx.doi.org/10.1016/j.earscirev.2004.06.003.
Leonard, M., 2010. Earthquake fault scaling: self-consistent relating of rupture length, width, average displacement, and moment release. Bull. Seismol. Soc. Am. 100 (5A), 1971–1988. http://dx.doi.org/10.1785/0120090189.
Mai, P.M., Beroza, G.C., 2000. Source scaling properties from finite-fault-rupture models. Bull. Seismol. Soc. Am. 90 (3), 604–615.
Main, I.G., Bell, A.F., Meredith, P.G., Geiger, S., Touati, S., 2012. The dilatancy–diffusion hypothesis and earthquake predictability. In: Healy, D., Butler, R.W.H., Shipton, Z.K., Sibson, R.H. (Eds.), Faulting, fracturing and igneous intrusion in the Earth's crust. Geol. Soc. London, Special Publications 367, pp. 215–230. http://dx.doi.org/10.1144/SP367.15.
Marone, C., 1998. Laboratory-derived friction laws and their application to seismic faulting. Annu. Rev. Earth Planet. Sci. 26, 643–696.
Mele, G., Di Luzio, E., Di Salvo, C., 2013. Mapping Moho depth variations in central Italy from PsMoho-P delay times: evidence of an E–W transition in the Adriatic Moho at 42-N latitude. Geochem. Geophys. Geosyst. 14, 3929–3938. http://dx.doi.org/10.1002/ggge.20235.
Meletti, C., Galadini, F., Valensise, G., Stucchi, M., Basili, R., Barba, S., Vannucci, G., Boschi, E., 2008. A seismic source zone model for the seismic hazard assessment of the Italian territory. Tectonophysics 450, 85–108.
Mirabella, F., Brozzetti, F., Lupattelli, A., Barchi, M.R., 2011. Tectonic evolution of a low-angle extensional fault system from restored cross-sections in the Northern Apennines (Italy). Tectonics 30, TC6002. http://dx.doi.org/10.1029/2011TC002890.
Montone, P., Mariucci, M.T., Pierdominici, S., 2012. The Italian present-day stress map. Geophys. J. Int. 189, 705–716.
Morellato, C., Redini, F., Doglioni, C., 2003. On the number and spacing of faults. Terra Nova 15, 315–321. http://dx.doi.org/10.1046/j.1365-3121.2003.00501.x.
Niemeijer, A., Marone, C., Elsworth, D., 2010. Frictional strength and strain weakening in simulated fault gouge: competition between geometrical weakening and chemical strengthening. J. Geophys. Res. 115, B10207. http://dx.doi.org/10.1029/2009JB000838.
Panza, G.F., Mura, C.L., Peresan, A., Romanelli, F., Vaccari, F., 2012. Seismic hazard scenarios as preventive tools for a disaster resilient society. Adv. Geophys. 53, 93–165.
Pauselli, C., Ranalli, G., Federico, C., 2010. Rheology of the Northern Apennines: lateral variations of lithospheric strength. Tectonophysics 484 (1–4), 27–35.
Petricca, P., Carafa, M.M.C., Barba, S., Carminati, E., 2013. Local, regional, and platescale sources for the stress field in the Adriatic and Periadriatic region. Mar. Pet. Geol. 42, 160–181. http://dx.doi.org/10.1016/j.marpetgeo.2012.08.005.
Pingue, F., De Natale, G., 1993. Fault mechanism of the 40 seconds subevent of the 1980 Irpinia (Southern Italy) earthquake from levelling data. Geophys. Res. Lett. 20 (10), 911–914.
Riguzzi, F., Crespi, M., Devoti, R., Doglioni, C., Pietrantonio, G., Pisani, A.R., 2012. Geodetic strain rate and earthquake size: new clues for seismic hazard studies. Phys. Earth Planet. Inter. 206–207, 67–75.
Riguzzi, F., Crespi, M., Devoti, R., Doglioni, C., Pietrantonio, G., Pisani, A.R., 2013. Strain rate relaxation of normal and thrust faults in Italy. Geophys. J. Int. 195, 815–820. http://dx.doi.org/10.1093/gji/ggt304.
Ruina, A., 1983. Slip instability and state variable friction laws. J. Geophys. Res. 88, 10359–10370.
Rutter, E.H., 1986. On the nomenclature of mode of failure transitions in rocks. Tectonophysics 122, 381–387.
Savage, J.C., Walsh, J.B., 1978. Gravitational energy and faulting. Bull. Seismol. Soc. Am. 68 (6), 1613–1622.
Schleicher, A.M., van der Pluijm, B.A., Warr, L.N., 2010. Nanocoatings of clay and creep of the San Andreas fault at Parkfield, California. Geology 38 (7), 667–670. http://dx.doi.org/10.1130/G31091.1.
Schlumberger, 2013. FMI-HD Microimager identifies vugs and fractures in high-resistivity carbonate, Permian Basin. http://www.slb.com/services/characterization/ geology/wireline/fullbore_formation_microimager_hd.aspx.
Scholz, C.H., 2002. The Mechanics of Earthquakes and Faulting. Cambridge University Press, Cambridge, New York (471 pp.).
Scholz, C.H., Contreras, J.C., 1998. Mechanics of continental rift architecture. Geology 26 (11), 967–970.
Schorlemmer, D., Wiemer, S., Wyss, M., 2005. Variations in earthquake-size distribution across different stress regimes. Nature 437, 22. http://dx.doi.org/10.1038/nature04094.
Shen, Y., 2002. Seismicity at the southern East Pacific Rise from recordings of an ocean bottom seismometer array. J. Geophys. Res. 107 (B12), 2368. http://dx.doi.org/10.1029/2001JB001742.
Sibson, R.H., 1974. Frictional constraints on thrust, wrench and normal faults. Nature 249, 542–544.
Sibson, R.H., 1990. Rupture nucleation on unfavorably oriented faults. Bull. Seismol. Soc. Am. 80 (6A), 1580–1604.
Sloan, R.A., Jackson, J.A., McKenzie, D., Priestley, K., 2011. Earthquake depth distributions in central Asia, and their relations with lithosphere thickness, shortening and extension. Geophys. J. Int. 185, 1–29. http://dx.doi.org/10.1111/j.1365-246X.2010.04882.x.
Wells, D.L., Coppersmith, K.J., 1994. New empirical relationships among magnitude, rupture length, rupture width, rupture area, and surface displacement. Bull. Seismol. Soc. Am. 84, 974–1002.
Yang, Z., Chen, W.-P., 2010. Earthquakes along the East African Rift system—a multi-scale, system-wide approach. J. Geophys. Res. 115, B12. http://dx.doi.org/10.1029/2009JB006779.
Zoback, M.D., Townend, J., 2001. Implications of hydrostatic pore pressures and high crustal strength for the deformation of intraplate lithosphere. Tectonophysics 336 (1), 19–30. http://dx.doi.org/10.1016/S0040-1951(01)00091-9.